Electric Load Classification by Binary Voltage–Current Trajectory Mapping

Liang Du, *Member, IEEE*, Dawei He, *Student Member, IEEE*, Ronald G. Harley, *Fellow, IEEE*, and Thomas G. Habetler, *Fellow, IEEE*

***Abstract*—Characterization of electric loads provides opportunities to incorporate detailed energy usage information into applications such as protection, efficiency certification, demand response, and energy management. This paper proposes a low computational cost, but yet accurate method, to extract signatures for load classification and characterization. Instead of utilizing digital signal processing and frequency-domain analysis, this paper abstracts the similarity of voltage–current (V–I) trajectories between loads and proposes to map V–I trajectories to a grid of cells with binary values. Graphical signatures can then be extracted for many applications. The proposed method significantly reduces the computational cost compared with existing frequency-domain signature extraction methods. Test results show that an average of over 99% of success rate can be achieved using the proposed signatures.**

***Index Terms*—Load classification, load identification, load signatures, nonintrusive load monitoring (NILM).**

I. Introduction

ELECTRIC loads in commercial and residential buildings consumed about 75% of total electricity in 2011 in the U.S. [1]. Global attention has been attracted to improve the efficiency, reliability, and functionality of building electric loads. Nonintrusive load monitoring (NILM) has been the major framework for monitoring energy consumption since 1990s [3]. Conventionally, the NILM framework focuses mainly on major loads such as heating, ventilation, and air conditioning systems.

Recently, NILM has been extended to plugged-in electric loads (PELs) (or miscellaneous electric loads in some contexts), i.e., loads with external power supply units [4]–[6]. Examples of PELs include consumer electronics as well as portable major loads such as portable refrigerators, washers, and driers. PELs are of special interests.

1) PELs currently account for more usage than any other single end-use service [7].
2) A large portion of this giant amount of electricity was wasted as vampire energy or standby power [8]. Proper PELs management can result in as much as 75% standby power savings [9] and 40 million tons of carbon emission reduction expected per year in U.S. [10].
3) PELs are more frequently installed, easily accessible, and controllable compared to nonportable electric loads [11].
4) PELs are more intelligent and networked in future.

To summarize, PELs possess great and unique potential to be efficiently managed as they can be directly controlled (e.g., turned ON/OFF) by switches in power strips, main sockets, and power outlets. For instance, Building America, by the U.S. Department of Energy, has started to identify and reduce electric loads consumption [12] and aims at 50% energy savings in new residential homes by 2015.

Within the NILM framework, a reliable and affordable method to identify the type, model, and status of an unknown load is a prerequisite (known as load identification). Many efforts have been devoted to the load identification problem. A comprehensive survey of existing solutions can be found in [2]. The performance of almost all existing load identification methods highly depends on the electrical signatures of each load, which are defined as "an electrical expression that a load device or appliance distinctly possesses" [13]. Typical signatures used in literature include RMS current value, total harmonic distortion (THD), power factor, harmonics, and transient power. These signatures require discrete or fast Fourier transformations (FFTs) on the current and/or voltage waveforms, which could be computationally expensive for applications with limited processor capability. To overcome this burden, this paper proposes a Fourier-transform free signature extraction algorithm which computationally costs far less.

Furthermore, it is shown in [14] that the fast development of front-end power supply design brings challenges to the load identification problem. Each type of PELs may have many different brands, models, and operating modes. Moreover, each type of PELs may be equipped with different front-end power supply topologies. Also, different types of PELs may be

Manuscript received September 1, 2014; revised December 3, 2014, February 12, 2015, and April 7, 2015; accepted May 24, 2015. Date of publication June 22, 2015; date of current version December 19, 2015. This work was supported in part by the U.S. Department of Energy National Energy Technology Laboratory under Award DE-EE0003911, and in part by the Eaton Corporation. Paper no. TSG-00868-2014.

L. Du was with the School of Electrical and Computer Engineering, Georgia Institute of Technology, Atlanta, GA 30332 USA. He is now with the Pressure Pumping and Chemistry Product Group, Schlumberger, Sugar Land, TX 77478 USA (e-mail: liang.du@ieee.org).

D. He and T. G. Habetler are with the School of Electrical and Computer Engineering, Georgia Institute of Technology, Atlanta, GA 30332 USA (e-mail: hedawei@gatech.edu; thabetler@ece.gatech.edu).

R. G. Harley is with the School of Electrical and Computer Engineering, Georgia Institute of Technology, Atlanta, GA 30332 USA, and also with the School of Engineering, University of KwaZulu-Natal, Durban, South Africa (e-mail: rharley@ece.gatech.edu).

Color versions of one or more of the figures in this paper are available online at http://ieeexplore.ieee.org.

Digital Object Identifier 10.1109/TSG.2015.2442225

equipped by similar power supply units [15]. These problems have not been well addressed in literature.

To handle the diversity within each type of PELs and the similarity between different types of PELs, a two-step framework is proposed in [16] to improve accuracy, reliability, and robustness. The first step is called load classification, in which all PELs are grouped into seven categories based on their most common front-end power supply topologies [14]. The second step is called in-category load identification. Within each category, operating principles of PELs with similar front-end power supply topology are considered for load identification [17], [18].

This paper proposes a novel set of computationally efficient but yet accurate signatures for load classification. The voltage–current (V–I) trajectories are first mapped to a grid of cells, each of which is assigned a binary value. A set of simple but yet efficient signatures can then be extracted directly from the mapped cell grid. Though the proposed features are mainly designed for load classification, they can be combined with existing in-category load identification methods such as support vector machines [15], supervised self-organizing maps (SSOMs) [16], and state-based features from long-term waveforms [18] to form a complete two-step load identifier. The proposed signatures can accurately assign an unknown load into one load category. Existing in-category identification methods can then determine its identity.

This paper is organized as follows. Section II introduces the load categories by front-end electronic circuit topology and typical V–I trajectories of loads in each category. Section III proposes an algorithm to map the V–I trajectories to a binary cell grid. Section IV presents a set of graphical signatures that can be extracted from the mapped cell grid and compares its computational cost with several widely used algorithms. Section V provides several test results with different scenarios. Finally, Section VI summarizes the conclusion of this paper.

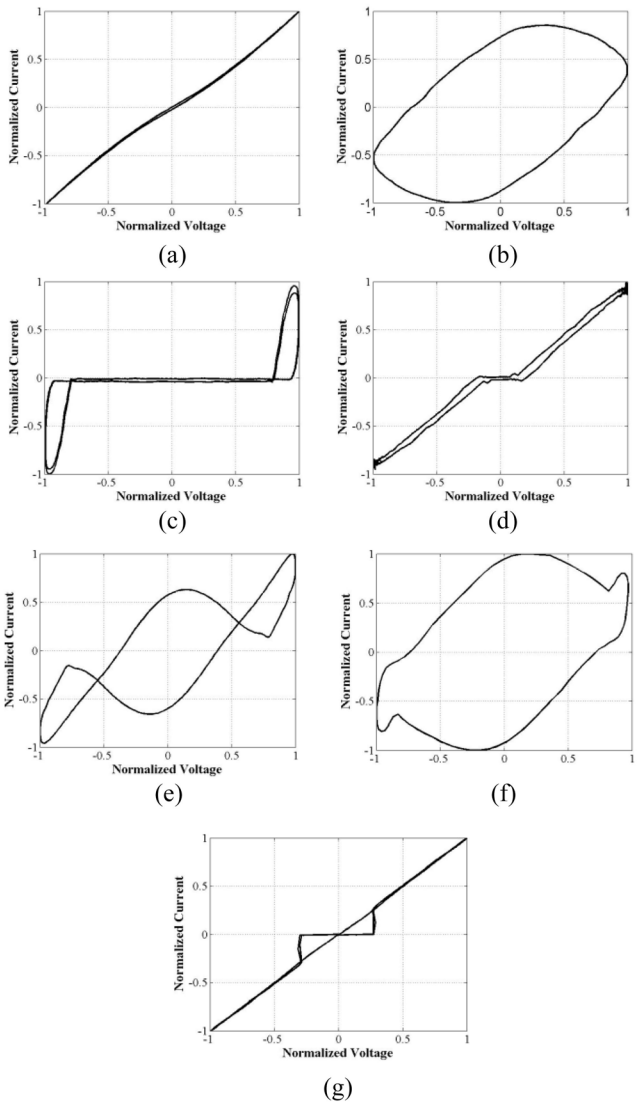

Fig. 1. Typical normalized V–I trajectories of seven load categories. (a) Category R. (b) Category X. (c) Category NP. (d) Category P. (e) Category M. (f) Category T. (g) Category PAC.

II. Electric Load Categories by Front-End Electronic Circuit Topology and Their Typical V–I Trajectories

It is more practical to first divide all PELs into categories and then extract common signatures for PELs in each category.

A. Electric Load Categories by Front-End Circuit Topology

A hierarchical taxonomy was proposed in [14] to divide PELs into the following seven categories.

1) *Resistive Load (Category R):* A category R load typically contains a resistance connected to the front-end terminal and there is no phase angle displacement between current and voltage.
2) *Reactive Loads (Category X):* A category X load typically contains an inductance directly connected to the front-end through a rectifier and there is a large phase displacement between current and voltage.
3) *Electronic Loads Without Power Factor Correction (Category NP):* A category NP load typically consists of a front-end EMI, a rectifier, a voltage or current filter, and a dc–dc converter. There is no phase angle displacement between current and voltage waveforms but the current waveform contains abundant harmonics.
4) *Electronic Loads With Power Factor Correction (Category P):* A category P load typically consists of a front-end EMI, a rectifier, a voltage regulator, a power factor correction module, and a dc–dc converter.
5) *Complex Structure Loads (Category M):* A category M load typically consists of multiple circuits supplied by independent front-end power supply units. As a result, the load current appears to be composed of currents from one or more of other categories.
6) *Linear Loads (Category T):* A category T load typically consists of a transformer, a rectifier, and other downstream electronics.
7) *Phase Angle Controllable Loads (Category PAC):* A category PAC load continuously adjusts its load current by controlling the firing angle of a thyristor.

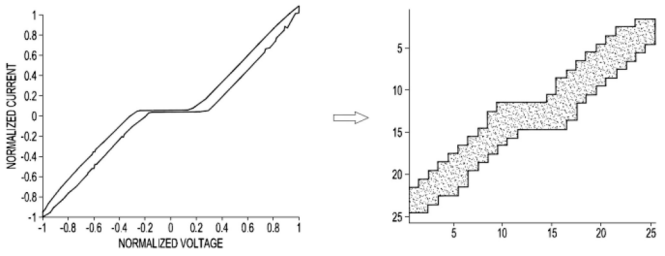

Fig. 2. Mapping V–I trajectory to a binary cell grid.

Note that, the categories T and PAC are no longer adopted in modern power supply industry, but these two categories are still included in this paper for completeness.

B. Typical V–I Trajectories of the Seven Load Categories

It is observed that the normalized V–I trajectories of PELs within each category share similar shapes, which can be used to represent PELs within each category. Furthermore, PELs of different categories possess quite different shapes of normalized V–I trajectories, which can be used to distinguish PELs from within different categories. Typical normalized V–I trajectories of the seven load categories are shown in Fig. 1.

A recent study summarizes that there are eight shape signatures that can be considered to describe the V–I trajectory: asymmetry, looping direction, area, curvature of the mean line, self-intersection, slope of middle segment, area of left and right segments, and peak of middle segment [13]. Similar results have been reported recently based on empirical studies [19]. However, calculating these signatures requires a large amount of computational effort. Furthermore, as shown in Section III, existing graphical signatures cannot effectively handle the diversity within each type of PELs and the similarity between different types of PELs.

III. Signature Extraction by Mapping V–I Trajectories to Cell Grids With Binary Values

A. Binary Mapping From V–I Trajectories

In order to effectively handle the difference between V–I trajectories of PELs within the same category, this paper proposes to first map the V–I trajectory to a grid of cells. Each cell is assigned a binary number. If the V–I trajectory cross though a cell, this cell is occupied by this V–I trajectory, assigned 1, and shown as a solid block as shown in Fig. 2.

The binary mapping algorithm is defined as follows.

1) *Load Voltage and Current Waveforms:* Assume that there are a total of K data points of the form (v_k, i_k), where $k = 1, \ldots, K$. Also, v_k and i_k are the voltage and current values of data point k, respectively.
2) Calculate

$$v_{\max} = \max v_k,\ v_{\min} = \min v_k$$
$$i_{\max} = \max i_k,\ i_{\min} = \min i_k$$
$$v_0 = \frac{1}{2}(v_{\max} + v_{\min}),\ \text{ and } i_0 = \frac{1}{2}(i_{\max} + i_{\min}). \quad (1)$$

3) Read input N, which defines the size of the grid in the horizontal direction.

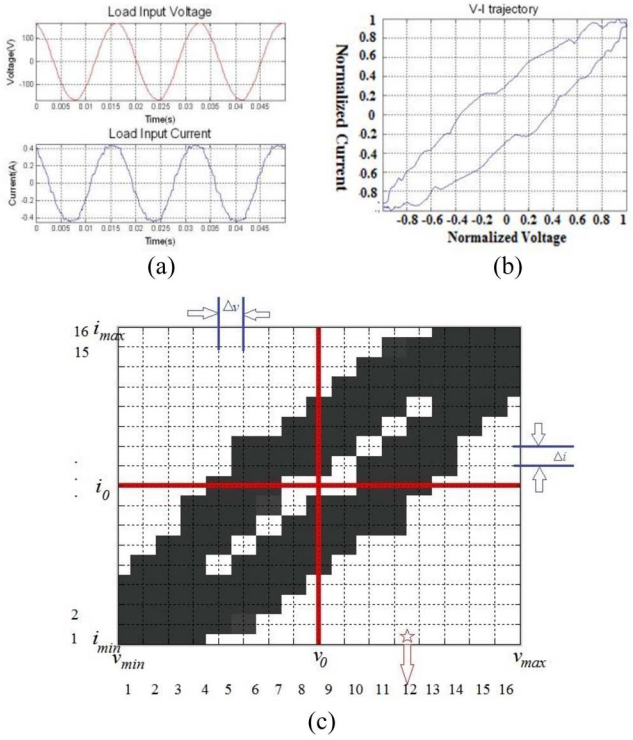

Fig. 3. Illustration of mapping a V–I trajectory to a binary cell grid. (a) Voltage and current waveforms of a fan. (b) Corresponding V–I trajectory. (c) Cell grid after mapping a V–I trajectory.

4) Calculate

$$\Delta v = \frac{v_{\max} - v_0}{N},\ \Delta i = \frac{i_{\max} - i_0}{N} \quad (2)$$

and generate two sequences

$$\{v_0 - N \cdot \Delta v, \ldots, v_0 - \Delta v, v_0 + \Delta v, \ldots, v_0 + N \cdot \Delta v\}$$

and

$$\{i_0 - N \cdot \Delta i, \ldots, i_0 - \Delta i, i_0 + \Delta i, \ldots, i_0 + N \cdot \Delta i\}$$

which both have $2N$ elements.

5) Define a $2N \times 2N$ cell grid. Cell (xth, yth) is assigned a positional value $(v_0 + \Delta\, v \cdot (x - N), i_0 + \Delta\, i \cdot (y - N))$ and a binary model value $B_{x,y}$ which is initialized to be 0.
6) Load half-cycle of data points, starting from the zero crossing point from negative to positive to another zero crossing point from positive to negative.
7) Start with the first data point (v_1^h, i_1^h) of all the data points loaded in step 6), and execute the following loop:

for every cell $(N + 1, y)$, $y = N + 1, N + 2, \ldots, 2N$
  if $(v_1^h - v_0) < \frac{\Delta v}{2}$ and $(i_1^h - (i_0 + (y - N) \cdot \Delta i)) < \frac{\Delta i}{2}$
    cell $(N + 1, y)$ is occupied and $B_{\Delta+1,y} = 1$;
   cell $(N + 1, y)$ is stored as the *winner* of(v_1^h, i_1^h);
    break;
  end
end

8) For the remaining data points from step 6), repeat step 7) by searching the eight adjacent cells of the previous winner.
9) Repeat step 7) for a predefined number of times.

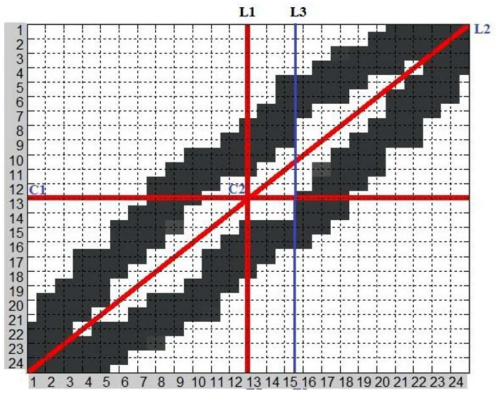

Fig. 4. Two key cells (C1 and C2) and three key lines (L1–L3).

The parameter N should be carefully chosen based on applications. If there are too many cells, the mapping may not effectively handle the variance of similar V–I trajectories. However, the mapped grid may not correctly represent the V–I trajectories if the number of cells is insufficient.

B. Illustration of Binary Mapping Algorithm

The following example illustrates the proposed mapping algorithm. Raw waveforms of a portable fan are shown in Fig. 3(a). The corresponding V–I trajectory and the mapped cell grid are shown in Fig. 3(b) and (c), respectively. The parameter N is 8 and thus the cell grid is of the size 16×16.

For this example

$$v_{\max} = 169.2 \text{ V}, v_{\min} = -168.3 \text{ V}$$
$$i_{\max} = 0.45 \text{ A}, i_{\min} = -0.44 \text{ A}$$
$$v_0 = 0.45 \text{ V}, i_0 = 0.05 \text{ A}$$
$$\Delta v = 21.1 \text{ V}, \Delta i = 0.05 \text{ A}.$$

To illustration, the (12th, 1st) cell marked by a star in Fig. 3(c) is selected as an example. It has the positional value $(0.45 + 4 \times 21.1, 0.05 + 4 \times 0.05) = (84.85, 0.25)$ and the binary model value 0 (i.e., not occupied).

IV. Signatures Extracted From the Binary Cell Grid

Besides reducing the variance in V–I trajectories of PELs within the same category, the mapping of V–I trajectories onto binary cell grids can also reduce the effect of distortion and preserve the graphical characteristics.

A. Load Signatures From V–I Trajectories Mapping

For each category of PELs, a novel set of signatures can be directly identified from the binary cell grid according to two key cells and three key lines, as shown in Fig. 4.

The following signatures identically represent PELs within category.

1) The binary value of the left horizontal cell $(1, N)$, marked as cell "C1." For instance, in Fig. 4 the binary model value $B_{1,12}$ of cell C1, i.e., cell (1, 12), is 0.

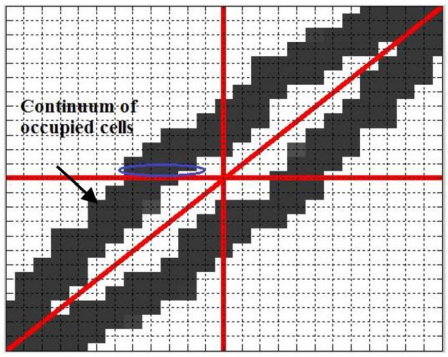

Fig. 5. Example of a continuum of occupied cells in the grid.

2) The binary value of the central cell (N, N), marked as cell "C2." For instance, in Fig. 4 the binary model value $B_{12,12}$ of cell C2, i.e., cell (12, 12), is 1.
3) The multiplication of the binary values of all anti-diagonal grid cells, i.e., all cells traversed by line "L2." This binary value indicates whether the V–I trajectory is linear. In Fig. 4, this value is 0 as some anti-diagonal cells are not occupied (and thus are of 0 value).
4) The number of continuums of occupied cells (i.e., with binary value 1) within all cells $(N, [1 : 2N])$, which indicates the number of intersections of the V–I trajectory and the base v_0 line (marked as line "L1").
   Note that, the notation $[1 : 2N]$ denotes all integers from 1 to N. Also, a continuum of occupied cells means a set of cells that are occupied and adjacent to one another in the grid. Fig. 5 shows that the number of continuums of occupied cells, instead of the number of occupied cells, makes the proposed PELs signature more robust to variations and measurement noise.
5) Whether there exist any self-crossing intersections of the V–I trajectory itself. Fig. 1(e) shows self-crossing intersections in the V–I trajectory for category M PELs. However, there are no self-crossing intersections in the V–I trajectory for PELs from categories R and X as shown in Fig. 1(a) and (b).
6) The number of intersections of the V–I trajectory with the $v_0 + 0.2N \times \Delta v$ line (marked as line "L3" in Fig. 4).

B. Determining the Number of Self-Crossing Intersections

It is suggested in [13] that the number of self-crossing intersections contained by a V–I trajectory could be related to the order of harmonics. However, self-crossing intersections can also be caused by loads in category M, i.e., loads with multiple independent front-end power supply units. Therefore, this paper proposes a general but yet low-cost algorithm to determine the number of self-crossing intersections contained in a V–I trajectory, as shown in Fig. 6.

The number of self-crossings contained in a V–I trajectory can be determined by the following steps.

1) Read half-cycle of data points $[0_-, 0_+]$, starting with the zero-crossing data point from negative to positive voltage values (denoted by 0_-) and ending with the zero-crossing data point from positive to negative voltage values (denoted by 0_+).

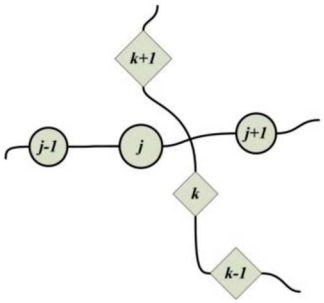

Fig. 6. Determining the number of self-crossing intersections.

2) For every data point $\boldsymbol{j}$ within the region $[0_-, \text{peak}_+]$, where peak_+ denotes the data point in $[0_-, 0_+]$ with the maximal positive voltage value, find the data point $\boldsymbol{k}$ whose voltage value is closest to point $\boldsymbol{j}$.
3) Denote a data point $\boldsymbol{j}$ with voltage value v_j and current value i_j by a vector $\underline{\boldsymbol{j}}$, check whether values of the current of the data point sequence $\{\underline{\boldsymbol{j}-1}, \underline{\boldsymbol{j}}, \underline{\boldsymbol{j}+1}\}$ and $\{\underline{\boldsymbol{k}-1}, \underline{\boldsymbol{k}}, \underline{\boldsymbol{k}+1}\}$ are monotonically increasing. If yes, go to step 4); if not, repeat step 3) and start with $\boldsymbol{j}+1$.
4) Check whether data points $\underline{\boldsymbol{k-1}} = (v_{k-1}, i_{k-1})$ and $\underline{\boldsymbol{k+1}} = (v_{k+1}, i_{k+1})$ are on different sides of the line determined by $\underline{\boldsymbol{j-1}} = (v_{j-1}, i_{j-1})$ and $\underline{\boldsymbol{j+1}} = (v_{j+1}, i_{j+1})$ using the following criterion:

$$\left\{\left(\underline{\boldsymbol{j+1}} - \underline{\boldsymbol{j-1}}\right) \times \left(\underline{\boldsymbol{j+1}} - \underline{\boldsymbol{k-1}}\right)\right\} \cdot \left\{\left(\underline{\boldsymbol{j+1}} - \underline{\boldsymbol{j-1}}\right) \times \left(\underline{\boldsymbol{j+1}} - \underline{\boldsymbol{k+1}}\right)\right\} < 0 \quad (3)$$

where $\times$ denotes the cross product and $\cdot$ denotes the dot product. In other words, for any $\boldsymbol{j}$ and $\boldsymbol{k}$, an instance when (3) is satisfied is considered as a self-crossing intersection.

C. Computational Complexity Analysis

Most existing load signatures are extracted from the harmonic spectra of the voltage and current waveforms, which require computing the discrete Fourier transformation (DFT) or the FFT and their inverses. Assume that voltage and current waveforms are given as

$$V(t) = \sum_{p=1}^{\infty} V_p \sin\left(p\omega_0 t + \delta_p\right) \quad (4)$$

$$I(t) = \sum_{p=1}^{\infty} I_p \sin\left(p\omega_0 t + \theta_p\right) \quad (5)$$

where ω_0 is the fundamental frequency, V_k and δ_k denote the magnitude and phase angle of the kth harmonic in voltage, and I_k and θ_k denote the magnitude and phase angle of the kth harmonic in current, respectively. The following steady-state load signatures [2], [20], [21] from the harmonic spectra are widely used in various load identification systems.

1) The RMS current I_{RMS}.
2) The THD in current

$$\text{THD}_I = \frac{\sqrt{\sum_{p=2}^{\infty} I_p^2}}{I_1} \cdot 100\%.$$

TABLE I
COMPARISON OF THE NUMBER OF REAL MULTIPLICATIONS AND REAL ADDITIONS NEEDED BY DIFFERENT ALGORITHMS

Algorithms	Goertzel	Radix-2 FFT	Binary mapping
	N-point data M DFT terms	N-point data	N-point data $L \times L$ cell grid
Complexity	$O(NM)$	$O(N \log_2 N)$	$O(N)$
Real multiplications	$(2N+4)M$	$2N \log_2 N$	~$4N$
Real additions	$(4N+4)M$	$2N \log_2 N$	~$8N$

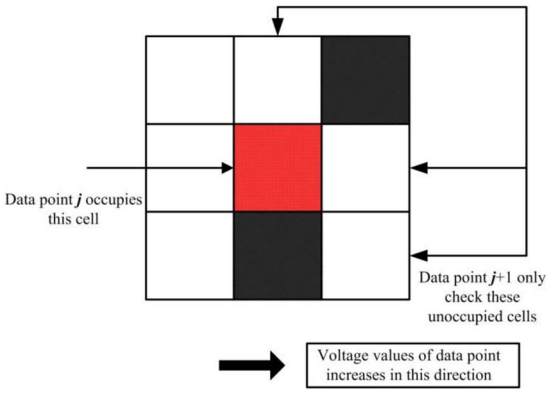

Fig. 7. Checking only adjacent unoccupied cells in one direction.

3) The power factor $\text{pf} = \cos(\delta_1 - \theta_1)/\sqrt{1 + \text{THD}_I^2}$, where δ_1 and θ_1 are the fundamental voltage and current angles.
4) The third and fifth harmonics (amplitude and phase).

Though many algorithms have been proposed to reduce the computational complexity of FFT and DFT [22], [23], they may still be computationally expensive for many NILM applications. The proposed load signatures greatly reduce the computational cost. Table I compares the number of real multiplications and additions needed by the proposed binary mapping method with two widely used algorithms.

1) Goertzel's algorithm, which converts the DFT equation into an equivalent form as a convolution and is widely used for calculating individual DFT terms [24].
2) Radix-2 FFT algorithm, which divides a DFT of size N into two interleaved DFTs of size $N/2$, greatly improves the computational efficiency, and is the simplest and most common form of FFT [25].

Determining values in (1) does not require much computational effort as data points are read half-cycle by half-cycle and ordered by voltage values. Each data point is only compared to adjacent unoccupied cells in one direction, as shown in Fig. 7. In the extreme case of only computing the first, third, and fifth harmonics in current, i.e., $M = 4$, the proposed algorithm still has computational advantages over other two algorithms. If a full harmonic spectrum is present, the proposed algorithm needs the same number of multiplications and additions as Goertzel's algorithm with $N = 4$. However, in practical cases N is much greater than 4.

TABLE II
EXPECTED SIGNATURES OF FIRST FIVE LOAD CATEGORIES

Category	signature 1	signature 2	signature 3	signature 4	signature 5
R	0	1	1	1	0
X	0	0	0	2	0
NP	1	1	0	1	0
P	0	1	0	1	0
M	0	X	0	2	1+

- where "X" means either 0 or 1 and "1+" means 1 or more.

TABLE III
TEST RESULTS OF FIRST FIVE LOAD CATEGORIES

Category	Total Number of Loads	Total Number of Tests	Total Number of Correct	Success Rate
R	6 (4 space heaters and 2 coffer makers)	600	597	99.5%
X	10 (5 fans, 1 water dispenser, and 4 refrigerators)	1000	991	99.1%
NP	15 (1 battery charger, 4 DVD players, 2 desktop computers, 7 LCD monitors, and 1 printer	1500	1493	99.5%
P	11 (5 LCD monitors, 3 LED monitor, 1 Plasma TV, 1 MFD, and 1 projector)	1100	1091	99.2%
M	4 microwave ovens	400	395	98.8%

V. NUMERICAL TEST RESULTS

In this section, the results of three tests are presented.

A. Data Collection

A database has been established to collect raw data [16], [26]. For accuracy and convenience, the sampling rate is set to be 30.72 kS/s. Lower sampling rates such as 7.68 and 3.84 kS/s are also tested and the results remain relatively the same. This database has a total of 627 sets of real-world data collected using a PCB module with current and voltage sensors and a set of data acquisition devices [26].

B. Supervised Self-Organizing Map

The self-organizing map (SOM) is an unsupervised artificial neural network trained by competitive learning. Du *et al.* [16], [26] proposed to extend the SOM to an SSOM for load classification and identification. The outputs of the SSOM consist of a number of clusters, each represents one load category. Due to space limit, the details of utilizing an SSOM for load identification are not included in this paper but can be found in [16], [26], and [27].

The performance of the SSOM classifier can be verified by cross-validation. The dataset is divided into two subsets. One is used to train the SSOM (called the training set), and the other is used to test its performance (called the testing set). Both subsets are labeled in the manner that every data point (i.e., a vector of signatures) is labeled by its actual category identity (i.e., which category it belongs to). For example, data points (i.e., vectors of signatures) extracted from raw waveforms of space heaters and coffee machines are all labeled as "category R." A correct classification is made if the SSOM-assigned category label of an input matches its actual category label.

TABLE IV
EXPECTED SIGNATURES OF ALL SEVEN LOAD CATEGORIES

Category	signature 1	signature 2	signature 3	signature 4	signature 5	signature 6
R	0	1	1	1	0	1
X	0	0	0	2	0	2
NP	1	1	0	1	0	1
P	0	1	X	1	0	1
M	0	X	0	2	1+	2
T	0	0	0	2	0	2
PAC	X	1	1	1	0	2

TABLE V
TEST RESULTS OF ALL SEVEN LOAD CATEGORIES

Target Load Category	Load Type	Total Models	Total Number of Tests	Success Rate (%)
NP	Battery charger	1	3000	83.4
	DVD player	4	3000	100
	Desktop computer	2	3000	99.8
	LCD monitor	7	3000	99.5
	Printer	1	3000	99.9
	Electronic circuit board	1	3000	98.7
P	LCD TV	8	3000	98.5
	LED TV	3	3000	99.2
	Plasma TV	2	3000	99
	Multi-function device	3	3000	93
	Projector	4	3000	99.9
M	Microwave oven	4	1800	99
R	Space heater	4	1800	93
	Coffee maker	2	1800	98
	Incandescent lamp	4	1800	99.2
	Electric skillet	2	1800	98.6
T	Stapler	1	1800	98.9
	Adapter	5	1800	100
X	Fan	5	3600	98.5
	Refrigerator	4	3600	100
	Water dispenser	1	3600	100
	Shredder	2	3600	65
PAC	Lamp with Dimmer	1	1800	50

TABLE VI
COMPARISON OF PROPOSED SIGNATURES AND CONVENTIONAL SIGNATURES USING SSOM

Test Loads	Total Number of Loads	Total Number of Tests	Success rate by proposed signature	Success rate by existing signature
LCD TV	3	300	100%	100%
Set-top Box	4	400	100%	100%
Space Heater	2	200	99%	96%
Laptop	2	200	99%	98.7%
LED TV	2	200	99%	100%
Microwave Oven	4	400	92%	91%
Desktop	2	200	97%	47%
Bluetooth Charger	1	100	99%	66.4%
Multi-Functional Device	3	300	100%	76.8%
LED Light	1	100	99%	96%

C. Test on Five Major Load Categories

As discussed in Section II-A, the first five load categories cover the majority of existing PELs. Thus, in this test the success rates of classifying loads from the first five load categories are presented. The proposed signatures are expected to have values in Table II.

For each category, a number of PELs have been tested and each PEL has been tested 100 times independently. The results are shown in Table III.

To summarize, the proposed signatures achieved an average of over 99% of classification success rate. The classification of category M PELs, i.e., loads with multiple independent front-end power supply units, has the lowest accuracy. This is mainly due to the wide diversity of loads in this category.

D. Test on All Seven Load Categories

In this test, all seven load categories are considered. The proposed signatures are expected to have values in Table IV.

A total of 75 sets of PELs (of 23 types) are tested. Results are presented in Table V.

PELs in category PAC are sometimes mistakenly categorized as category R due to the similarity between normalized V–I trajectories from these two categories.

To summarize, the proposed signatures combined with SSOM can achieve an average of over 99% (95%, respectively), classification success rate for major five (all, respectively) load categories.

E. Comparison of Proposed Signatures and Conventional Signatures Using SSOM

This test aims at comparing the performance of the SSOM used with proposed signatures against with conventional signatures defined in Section IV-C. In other words, the comparison is performed on the same dataset using the same method (i.e., SSOM). The same database from previous example is used to train a 50-by-50 SSOM and a total of 30 sets of PELs (of 13 types) are tested. For each testing dataset, 100 V–I trajectories are selected and mapped to a 256-by-256 cell grid. The comparison is shown in Table VI.

Table VI shows that the proposed signatures achieved higher load classification success rates compared to conventional signatures from harmonic analysis.

VI. CONCLUSION

This paper has proposed a low computational cost but yet accurate algorithm to extract signatures for load classification. Instead of utilizing Fourier transformations and frequency domain analysis, this paper abstracted the similarity of V–I trajectories between loads and proposed how to map V–I trajectories to a grid with binary cell values. Graphical signatures can then be extracted. The proposed method significantly reduces computational cost compared to existing frequency-domain signature extraction methods. Test results showed that an average success rate of more than 99% can be achieved using the proposed signatures.

ACKNOWLEDGMENT

This paper was prepared as an account of work sponsored by an agency of the United States Government. Neither the United States Government nor any agency thereof, nor any of their employees, makes any warranty, express or implied, or assumes any legal liability or responsibility for the accuracy, completeness, or usefulness of any information, apparatus, product, or process disclosed, or represents that its use would not infringe privately owned rights. Reference herein to any specific commercial product, process, or service by trade name, trademark, manufacturer, or otherwise does not necessarily constitute or imply its endorsement, recommendation, or favoring by the United States Government or any agency thereof. The views and opinions of authors expressed herein do not necessarily state or reflect those of the United States Government or any agency thereof.

REFERENCES

[1] "Annual Energy Review 2011," Dept. Energy, Energy Inf. Admin., Washington, DC, USA, Tech. Rep. EIA-0384, 2012.
[2] Y. Du, L. Du, B. Lu, R. G. Harley, and T. G. Habetler, "A review of identification and monitoring methods for electric loads in commercial and residential buildings," in *Proc. IEEE Energy Convers. Conf. Expo.*, Atlanta, GA, USA, Sep. 2010, pp. 4527–4533.
[3] G. W. Hart, E. C. Kern, and F. C. Schweppe, "Non-intrusive appliance monitor apparatus," U.S. Patent 4 858 141, Aug. 15, 1989.
[4] K. McKenney, M. Guernsey, R. Ponoum, and J. Rosenfeld, "Commercial miscellaneous electric loads: Energy consumption characterization and savings potential in 2008 by building type," TIAX LLC, Lexington, MA, USA, Tech. Rep. D0498, May 2010.
[5] M. Zeifman and K. Roth, "Non-intrusive appliance load monitoring: Review and outlook," *IEEE Trans. Consum. Electron.,* vol. 57, no. 1, pp. 76–84, Feb. 2011.
[6] Z. Zhang *et al.*, "Training-free non-intrusive load monitoring of electric vehicle charging with low sampling rate," in *Proc. 40th Annu. Conf. IEEE Ind. Electron. Soc.,* Richardson, TX, USA, Aug. 2014, pp. 5419–5425.
[7] U.S. Energy Information Administration. (2007). *Miscellaneous Electricity Services in the Buildings Sector*. [Online]. Available: http://www.eia.gov/oiaf/aeo/otheranalysis/mesbs.html
[8] J. A. Roberson *et. al.*, "After-hours power status of office equipment and energy use of miscellaneous plug-load equipment," Lawrence Berkeley Nat. Lab., Univ. California, Berkeley, CA, USA, Tech. Rep. LBNL-53729R, Jan. 2004.

[9] *Lawrence Berkeley National Laboratory: Standby Power Home Page*. [Online]. Available: http://standby.lbl.gov/
[10] C. D. Barley, C. Haley, R. Anderson, and L. Pratsch, "Building America system research plan for reduction of miscellaneous electrical loads in zero energy homes," Nat. Renew. Energy Lab., Golden, CO, USA, Tech. Rep. NREL/TP-550-43718, Nov. 2008.
[11] *Commercial and Residential Sector Miscellaneous Electricity Consumption: Y2005 and Projections to 2030*, TIAX LLC, Cambridge, MA, USA, 2006.
[12] *Building America: Resources for Energy Efficient Homes*. [Online]. Available: http://www1.eere.energy.gov/buildings/building_america/
[13] H. Y. Lam, G. S. K. Fung, and W. K. Lee, "A novel method to construct taxonomy electrical appliances based on load signatures," *IEEE Trans. Consum. Electron.,* vol. 53, no. 2, pp. 653–660, May 2007.
[14] D. He, L. Du, Y. Yang, R. G. Harley, and T. G. Habetler, "Front-end electronic circuit topology analysis for model-driven classification and monitoring of appliance loads in smart buildings," *IEEE Trans. Smart Grid,* vol. 3, no. 4, pp. 2286–2293, Dec. 2012.
[15] L. Du, Y. Yang, D. He, R. G. Harley, and T. G. Habetler, "Support vector machine based methods for non-intrusive identification of miscellaneous electric loads," in *Proc. 38th Annu. Conf. IEEE Ind. Electron. Soc.*, Montreal, QC, Canada, Oct. 2012, pp. 4866–4871.
[16] L. Du *et al.*, "Self-organizing classification and identification of miscellaneous electric loads," in *Proc. IEEE Power Energy Soc. Gen. Meeting*, San Diego, CA, USA, Jul. 2012, pp. 1–6.
[17] D. He, L. Du, R. Harley, T. Habetler, and Y. Yang, "Electronic circuit survey for office load monitoring and identification," in *Proc. Energy Convers. Congr. Expo. (ECCE)*, Raleigh, NC, USA, Sep. 2012, pp. 1228–1232.
[18] L. Du, Y. Yang, D. He, R. G. Harley, and T. G. Habetler, "Feature extraction for load identification using long-term operating waveforms," *IEEE Trans. Smart Grid,* vol. 6, no. 2, pp. 819–826, Mar. 2015.
[19] T. Hassan, F. Javed, and N. Arshad, "An empirical investigation of V–I trajectory based load signatures for non-intrusive load monitoring," *IEEE Trans. Smart Grid*, vol. 5, no. 2, pp. 870–878, Mar. 2014.
[20] J. Liang, S. Ng, G. Kendall, and J. Cheng, "Load signature study—Part I: Basic concept, structure, and methodology," *IEEE Trans. Power Del.*, vol. 25, no. 2, pp. 551–560, Apr. 2010.
[21] F. Sultanem, "Using appliance signatures for monitoring residential loads at meter panel level," *IEEE Trans. Power Del.*, vol. 6, no. 4, pp. 1380–1385, Oct. 1991.
[22] C. Van Loan, *Computational Frameworks for the Fast Fourier Transform*. Philadelphia, PA, USA: SIAM Press, 1992.
[23] J. S. Walker, *Fast Fourier Transforms.* Boca Raton, FL, USA: CRC Press, 1996.
[24] A. V. Oppenheim and R. W. Schafer, *Discrete-Time Signal Processing*, 3rd ed. New York, NY, USA: Pearson, 2009.
[25] J. G. Proakis and D. K. Manolakis, *Digital Signal Processing: Principles Algorithms and Applications*, 4th ed. Englewood Cliffs, NJ, USA: Prentice Hall, 2006.
[26] L. Du, J. A. Restrepo, Y. Yang, R. G. Harley, and T. G. Habetler, "Nonintrusive, self-organizing, and probabilistic classification and identification of plugged-in electric loads," *IEEE Trans. Smart Grid*, vol. 4, no. 3, pp. 1371–1380, Sep. 2013.
[27] H. Chen, A. R. Iyer, R. G. Harley, and D. Divan, "Dynamic grid power routing using controllable network transformers (CNTs) with decoupled closed-loop controller," *IEEE Trans. Ind. Appl.*, vol. 51, no. 3, pp. 2361–2372, May/Jun. 2014.

Liang Du (S'09–M'13) received the Ph.D. degree in electrical and computer engineering from the Georgia Institute of Technology, Atlanta, GA, USA, in 2013.

He was a Summer Intern with Eaton Corporation Innovation Center, Milwaukee, WI, USA; Mitsubishi Electric Research Laboratories, Cambridge, MA, USA; and Philips Research North America, Briarcliff Manor, NY, USA, in 2011, 2012, and 2013, respectively. He is currently an Electrical Engineer with Schlumberger, Sugar Land, TX, USA.

Dawei He (S'10) was born in Jilin Province, China. He received the B.Eng. degree in electrical engineering from Tsinghua University, Beijing, China. He is currently pursuing the Ph.D. degree with the Georgia Institute of Technology, Atlanta, GA, USA.

Ronald G. Harley (M'77–SM'86–F'92) received the M.Sc.Eng. degree (cum laude) in electrical engineering from the University of Pretoria, Pretoria, South Africa, in 1965, and the Ph.D. degree from the University of London, London, U.K., in 1969.

In 1971, he was appointed as the Chair of Electrical Machines and Power Systems, University of KwaZulu-Natal, Durban, South Africa. He is currently a Regents' Professor and the Duke Power Company Distinguished Professor with the School of Electrical and Computer Engineering, Georgia Institute of Technology, Atlanta, GA, USA. He has published over 600 papers and presented several keynote papers around the world. He holds eight U.S. patents.

Dr. Harley was a recipient of the Cyril Veinott Electromechanical Energy Conversion Award from the IEEE Power Engineering Society for Outstanding Contributions to the Field of Electromechanical Energy Conversion in 2005, and the IEEE Richard H. Kaufmann Field Award with citation for Contributions to Monitoring, Control, and Optimization of Electrical Processes Including Electrical Machines and Power Networks in 2009. He is a Fellow of the Institution of Engineering and Technology, U.K., and the Royal Society in South Africa, and a Member of the Academy of Science in South Africa.

Thomas G. Habetler (S'85–M'89–SM'92–F'02) received the B.S. and M.S. degrees in electrical engineering from Marquette University, Milwaukee, WI, USA, in 1981 and 1984, respectively, and the Ph.D. degree from the University of Wisconsin–Madison, Madison, WI, in 1989.

From 1983 to 1985, he was a Project Engineer with the Electro-Motive Division, General Motors, La Grange, IL, USA. Since 1989, he has been with the School of Electrical and Computer Engineering, Georgia Institute of Technology, Atlanta, GA, USA, where he is currently a Professor of Electrical Engineering. His current research interests include electric machine protection and condition monitoring, switching converter technology, and drives.

Dr. Habetler was an inaugural recipient of the IEEE Power Electronics Society Diagnostics Achievement Award, the EPE-PEMC Outstanding Achievement Award, the 2012 IEEE Power Electronics Society Harry A. Owen Distinguished Service Award, the 2012 IEEE Industry Application Society Gerald Kliman Innovator Award, and one transaction and four conference prize paper awards from the IEEE Industry Applications Society. He has served on the IEEE Board of Directors as the Division II Director and the Technical Activities Board, as a Member and Geographic Activities Board, and as a Director of IEEE-USA. He was the President of the Power Electronics Society.